RESEARCH ARTICLE
SPACE PHYSICS: IONOSPHERIC PHYSICS

Earth and Planetary Physics
6: 529–535, 2022
doi: 10.26464/epp2023001

Electron acceleration by Langmuir turbulence in ionospheric heating

MoRan Liu, Chen Zhou*, and Ting Feng

Department of Space Physics, School of Electronic Information, Wuhan University, Wuhan 430072, China

Key Points:

- Electron acceleration by Langmuir turbulence in ionospheric heating is simulated by two models: a general two-fluid method with the Fokker–Planck equation and the Vlasov–Poisson system.
- The significant acceleration of electrons corresponds to the extension of the wavenumber spectrum, which is caused by Langmuir turbulence.
- The time evolution of electron holes in phase space at the same spatial scale as the Langmuir wave is presented by means of the Vlasov–Poisson code.

Citation: Liu, M. R., Zhou, C., and Feng, T. (2022). Electron acceleration by Langmuir turbulence in ionospheric heating. *Earth Planet. Phys.*, *6*(6), 529–535. http://doi.org/10.26464/epp2023001

Abstract: In this study, we investigate the generation of parametric decay instability, Langmuir turbulence formation, and electron acceleration in ionospheric heating via a two-fluid model using the Fokker–Planck equation and Vlasov–Poisson system simulations. The simulation results of both the magnetofluid model and the kinetic model demonstrate the dynamics of electron acceleration. Further, the results of the Vlasov–Poisson simulations suggest the formation of electron holes in phase space at the same spatial scale as the Langmuir wave, which are shown to be related to electron acceleration. In addition, electron acceleration is enhanced through the extension of the wavenumber spectrum caused by strong Langmuir turbulence, leading to more electron holes in phase space.

Keywords: electron acceleration; Langmuir turbulence; electron holes; parametric decay instability

1. Introduction

Ionospheric heating experiments are performed with high-power, high-frequency modification facilities (Djuth et al., 2005), and the F layer of the ionosphere is shown to be modified (Weinstock, 1975). A great variety of plasma phenomena are observed during these ionospheric modifications: artificial ionospheric layers (Sergeev et al., 2013), out-shifted plasma lines (Isham et al., 1999), high-frequency enhanced plasma lines (Carlson et al., 1972; Feng T et al., 2020), and stimulated electromagnetic emissions (Thidé et al., 1982; Wang X et al., 2019). For several decades, high-power radio waves have been well known to accelerate electrons, causing excited optical emissions and so-called artificial enhanced airglow (Djuth et al., 1999; Dang T et al., 2017). Djuth et al. (1999) also stated that the 630.0 nm emissions resulting from the inelastic collisional excitation of oxygen atoms require a minimum of only 1.96 eV for excitation. Further, Sergeev et al. (2013) observed that the accelerated electrons can ionize neutral gas if their energy exceeds 12–18 eV. Recently, Mishin et al. (2016) investigated the accelerated suprathermal electrons and descending artificial plasma layers excited by plasma turbulence.

Correspondence to: C. Zhou, chenzhou@whu.edu.cn
Received 30 MAY 2022; Accepted 12 AUG 2022.
Accepted article online 02 SEP 2022.

As early as 1971, Perkins and Flick proposed the theory that electrons are accelerated in ionospheric modifications, which are thought to be caused by parametric decay instability (PDI; Weinstock and Bezzerides, 1974). Parametric decay instability is one of the most important physical processes in ionospheric heating (Perkins et al., 1974), in which Langmuir waves and ion-acoustic waves can be excited just below the reflection region of ordinary (O-mode) polarization pump waves and directly observed as plasma lines and ion lines in incoherent scatter radar spectra (Robinson, 1989). Two indispensable conditions are needed for PDI stimulation: one is the PDI excited threshold (Bryers et al., 2013); another is the frequency and wavevector matching conditions $\omega_p = \omega_L + \omega_{IA}$ and $\boldsymbol{k}_p = \boldsymbol{k}_L + \boldsymbol{k}_{IA}$, where p, L, and IA denote pump waves, Langmuir waves, and ion-acoustic waves, respectively. Therefore, PDI is also called a three-wave interaction governed by the matching conditions (Fejer, 1979). If the two conditions mentioned above are both satisfied, the secondary PDI can be excited, in which the Langmuir wave decays into a daughter Langmuir wave and an ion-acoustic wave as a pump wave, namely, initiating a cascade process. This cascade process can subsequently induce Langmuir turbulence (LT), which can effectively accelerate ionospheric electrons (Isham et al., 1999). Eliasson and Stenflo (2008) have presented a generalized Zakharov model for electron acceleration. In that model, the PDI process and LT generation are studied by a two-fluid model, and electron acceler-

ation is calculated by the quasilinear diffusion coefficient. Recently, Najmi et al. (2017) also presented the electron acceleration near the upper hybrid resonance height by using a combination of Vlasov and test particle simulations.

Fluid and kinetic models are widely used to investigate the formation and dynamics of nonlinear processes excited in ionospheric heating (Eliasson and Shukla, 2006), in which LT can further lead to the formation and development of electron holes. An electron hole is a vortex distribution assigned to a population of trapped electrons. Eliasson and Shukla (2004) added perturbation to the initial condition for electron holes and found that they are attracted by ion density maxima but repelled by ion density minima by means of the Vlasov code.

Even though the knowledge of electron acceleration in ionospheric heating has been a subject of intense research in the past few decades, details of the time evolution remain to be understood. Unlike the research mentioned above, in this paper, we investigate electron acceleration by LT via the two-fluid model with the Fokker–Planck equation to examine electron acceleration via the effective diffusion coefficient and the Vlasov–Poisson code. Further, the simulation results of the Vlasov–Poisson system will help in understanding the nonlinear dynamics of electron holes, which will provide a potential explanation for electron acceleration by LT.

2. Electron Acceleration in the Two-Fluid Model for PDI

First, the two-fluid model presented here is utilized to analyze the excitation of PDI and the subsequent LT in ionospheric heating. We assume that a large-amplitude electromagnetic wave is injected vertically into the ionosphere and that the constant geomagnetic field $\boldsymbol{B}_0$ is considered. In the vertical z direction, electromagnetic wave propagation is governed by Maxwell equations with a Coulomb gauge. We separate the process into high-frequency equations (Equations (1a) and (1b)) and low-frequency equations (Equations (2a) and (2b)), referring to the model presented by Eliasson and Stenflo (2008). The difference between Eliasson's model and our model is that the slowly varying high-frequency field is obtained by averaging the electric field $\bar{\boldsymbol{E}}_h$ over a fast timescale instead of the slowly varying envelope of the high-frequency field $\tilde{\boldsymbol{E}}_h$ (Eliasson, 2008). Ponderomotive force is considered in the ion momentum in Equation (2),

$$\frac{\partial n_{eh}}{\partial t} = -\frac{\partial n_s v_{ezh}}{\partial z}, \tag{1a}$$

$$\frac{\partial \boldsymbol{v}_{eh}}{\partial t} = -\frac{\mathrm{e}}{m_e}[\boldsymbol{E}_h + \boldsymbol{v}_{eh} \times \boldsymbol{B}_0] - \frac{3v_{Te}^2}{n_e}\frac{\partial n_{eh}}{\partial z}\boldsymbol{z} - \upsilon_e \boldsymbol{v}_{eh}, \tag{1b}$$

$$\frac{\partial n_s}{\partial t} = -\frac{\partial (n_0 v_s)}{\partial z}, \tag{2a}$$

$$\frac{\partial v_s}{\partial t} = -{C_s}^2\frac{\partial n_s}{\partial z} - \upsilon_i v_s - \frac{1}{4}\frac{e^2}{m_i m_e \omega_0^2}\frac{\partial \left|\tilde{E}_h\right|^2}{\partial z}, \tag{2b}$$

where n is the density, v is the velocity, m is the mass of the particle, z is the vertical spatial coordinate, subscripts h and s represent the high-frequency process and the low-frequency process, subscripts e and i represent electrons and ions, $v_{Te} = (k_B T_e/m_e)^{1/2}$ is the electron thermal speed and $C_s = [k_B(T_e + 3T_i)/m_i]^{1/2}$ is the ion-acoustic speed, k_B is Boltzmann's constant, and T_e and T_i are the electron and ion temperatures. The oxygen ions are assumed to be immobile in high-frequency equations. The effect of the geomagnetic field on ions is neglected because of the large mass of ions compared with that of electrons (m_i/m_e = 29,500). Quasi-neutrality is assumed in the low-frequency equations.

The simulation parameters are as follows. The altitude range is 200–320 km. The ionospheric electron density profile is assumed to have a Gaussian shape with the formula of $n_0(z) = n_{\max}\exp[-(z - z_{\max})^2/L^2]$, where $n_{\max} = 1.436 \times 10^{11}$ m^{-3} is the electron density at the F_2 peak located at $z_{\max}$ = 300 km, and L = 31.62 km is the ionospheric scale length. The pump frequency is set as f_h = 3.2 MHz, which is smaller than the critical frequency f_0F_2 = 3.41 MHz. The pump wave is ordinarily polarized (O-mode) and the initial electric field is set to be E_0 = 1 V/m. The electron temperature T_e and the ion temperature T_i are both 2,320 K (0.2 eV). The electron and ion collision frequencies are set as the typical values of $\upsilon_e = 10^3$ s^{-1} and $\upsilon_i = 2 \times 10^3$ s^{-1}. The geomagnetic field is $\boldsymbol{B} = B_0[\boldsymbol{x}\cos(\theta) - \boldsymbol{z}\sin(\theta)]$, where B_0 is the geomagnetic field strength at ionosphere height $B_0 = 4.8 \times 10^{-5}$ T in the case of the EISCAT (European Incoherent Scatter Scientific Association) heating facility in Tromsø, Norway. The corresponding geomagnetic inclination θ is about 78.1°.

Figure 1 shows the simulation results at time t = 15,000 f_h^{-1}. The standing wave pattern of the electric field can be seen marginally below the reflection height. Between 287.5 and 287.7 km, small-scale Langmuir waves can be seen, and their maximum magnitude reaches 50 V/m. In addition, Langmuir cavitons can be found between 287.55 and 287.56 km, which are derived from ion density cavities trapping Langmuir waves. Figure 1 presents the initial stage of PDI in which the wave–particle interaction can accelerate the electrons by resonant effect. In the PDI process, Langmuir waves are excited, which could consequently transfer energy to electrons because of Landau damping. With the simulation results described above, the electron acceleration is investigated by a Fokker–Planck equation with effective diffusion coefficients calculated from the Langmuir wave spectrum as shown in Equation (3) (Eliasson et al., 2012):

$$\frac{\partial f_e}{\partial t} + v\frac{\partial f_e}{\partial z} = \frac{\partial}{\partial v}\left(D(v)\frac{\partial f_e}{\partial t}\right), \tag{3}$$

where f_e is the velocity space distribution, $D(v)$ is the diffusion coefficient calculated by

$$D(v) = \frac{\pi e^2}{m_e^2}\frac{W_k\left(\omega, \frac{\omega}{v}\right)}{|v|}, \tag{4}$$

where $W_k\left(\omega, \frac{\omega}{v}\right) = \Delta E^2/\Delta k$ is the spectral energy density of the electric field per wavenumber Δk, and ΔE^2 is the differential squared electric field. The simulated Langmuir wave spectra obtained in the height range of 287.5–287.7 km, which are shown in Figure 1, are taken to solve Equation (4). The initial electron distribution is assumed to be a Maxwell distribution.

Figure 2 shows the spectral energy density $W_k\left(\omega, \frac{\omega}{v}\right)$, the energy of the electric field, the spatially $E_k = \int_{-\infty}^{\infty} W_k \mathrm{d}k$, the spatially aver-

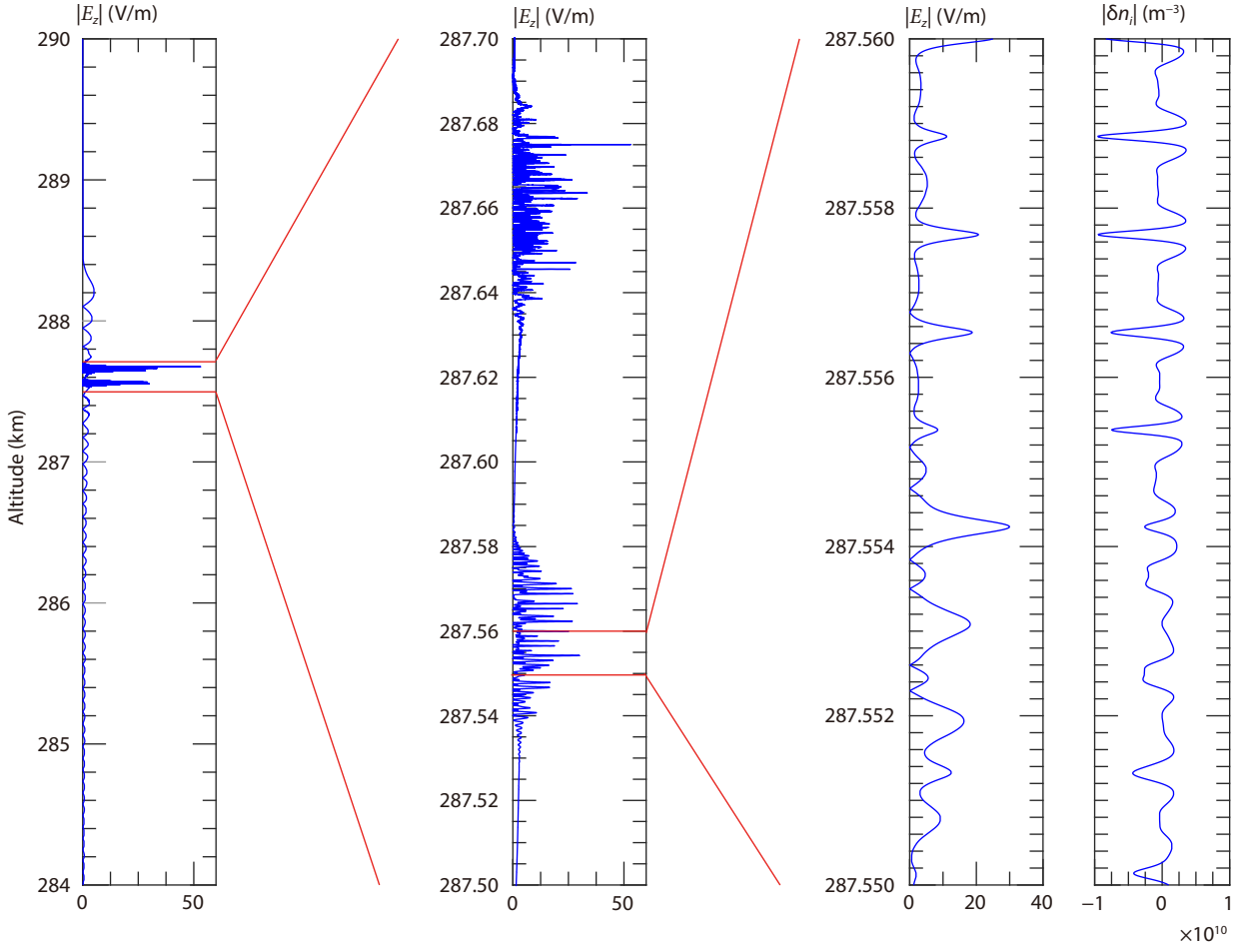

Figure 1. Simulation results of the parallel electric field and ion density structures at time t = 15,000 f_h^{-1}.

aged electron distribution <f_e>, and the spatial electron temperature <T_e> versus time t, where T_e is calculated by

$$T_e = \frac{\int_{-\infty}^{\infty} v^2 f_e \mathrm{d}v}{\int_{-\infty}^{\infty} f_e \mathrm{d}v} - \left[\frac{\int_{-\infty}^{\infty} v f_e \mathrm{d}v}{\int_{-\infty}^{\infty} f_e \mathrm{d}v}\right]^2. \quad (5)$$

At t = 10,000 f_h^{-1}, a significant enhancement of the Langmuir wave amplitude (compared with the standing waves) at k = 0.8/(2π) m^{-1} can be found, as shown in Figure 2a, which demonstrates the excitation of small-scale waves (wavelength of 1.125 m) in the initial PDI stage. In this stage, the pump wave decays into the daughter Langmuir wave, which will become a mother wave and decay. This is the so-called cascade process. Afterward, the spectrum is enhanced at integer multiples of k, that is, 2k and 3k. The appearance and enhancement of the spectral amplitude at discrete k indicate the generation of the cascade. Note that because of the generation of ion cavities, this cascade illustrates the energy enhancements at discrete wavenumbers instead of continuous ones, as presented in previous literature (Hanssen et al., 1992). The enhanced spectra at integer multiples of k reveal the existence of harmonic cavitons. Changes in the energy E_k, the electron distribution <f_e>, and the electron temperature <T_e> are evident until the LT stage begins at about t = 12,500 f_h^{-1}. The enhanced spectrum expands to larger k = 10/(2π) m^{-1}, which indicates the collapse of cavitons and the generation of strong LT (DuBois et al., 1988), and E_k begins to increase rapidly with time. In Figure 2c, the tail enhancement of the electron distribution is proof that electrons are accelerated in the LT stage, during which the corresponding <T_e> rises versus time. In Figure 2a, the wavenumber spectra are continuously enhanced during the LT period, and after about t = 17,500 f_h^{-1}, the enhanced spectrum narrows. The electric field energy decreases until it reaches a steady state at t = 22,500 f_h^{-1}. Meanwhile, the enhanced spectrum width stabilizes and the electron temperature is saturated. The electron temperature increases to about 5.0 eV in this simulation.

Our simulation results show that the waves with limited k in the initial PDI stage do not accelerate electrons effectively. The generation of LT leads to the extensive wavenumber spectrum enhancement, and the corresponding diffusion coefficient will increase to a broader velocity space. The pump energy is injected into large-scale (small-wavenumber) Langmuir waves, which transfer parts of the energy to small-scale waves. Electrons absorb energy from electrostatic waves in the LT process by the wave–particle resonant effect. Consequently, the energy of electrostatic waves dissipates into smaller scale waves because the viscosity contributes to the saturation stage.

Figure 3 shows the power spectra of the electric field E_z and the corresponding diffusion coefficients at three moments (t =

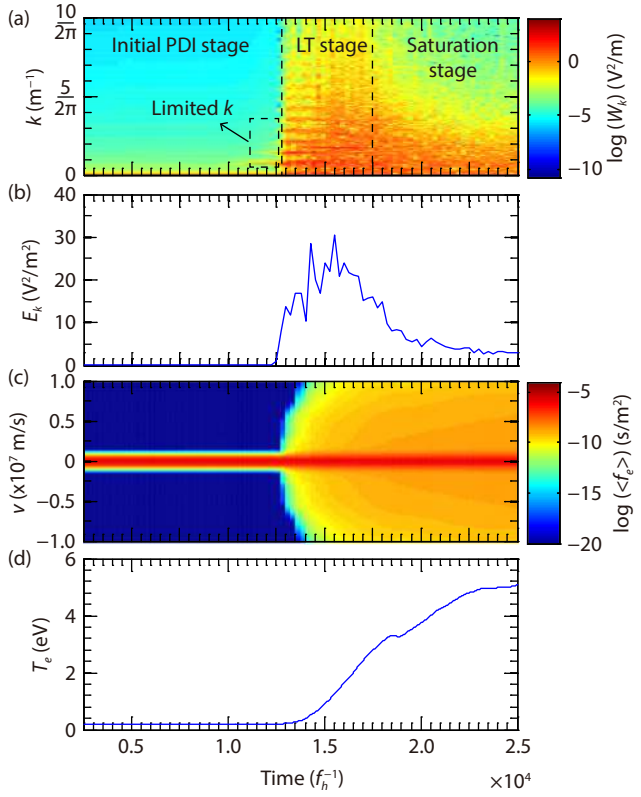

Figure 2. The time evolutions of (a) the spectral energy density, (b) the energy of electric field E_k, (c) the spatially averaged electron distribution, and (d) the spatially averaged electron temperature. PDI, parametric decay instability; LT, Langmuir turbulence.

12,500 f_h^{-1}, 15,500 f_h^{-1}, 22,500 f_h^{-1}) which represent the typical points in the initial PDI stage. LT stage, and saturation stage, respectively. The power spectra in the top row appear to be power-law shapes. In the LT stage (middle column in Figure 3), the electric field generally fits to a double power-law spectrum well, with the slope of the red fitting line $\beta = -2.054$ below the break at $k = 3$ m^{-1} and with the index $\beta = -6.12$ above the break. The wavenumber $k = 3$ m^{-1} corresponds to the wavelength of 0.3 m, which is close to the scale length of the ion cavity. The index $\beta = -2.054$ close to the Kolmogorov power-law index indicates that turbulence occurs within the ion cavities. The corresponding diffusion coefficient at the LT stage is much larger than at the other two stages; therefore, we can observe the most evident electron acceleration in the LT stage in Figure 2. The processes presented above indicate that ion cavities play an important role in electron acceleration.

3. Electron Acceleration in the Vlasov–Poisson System

The two-fluid model presents the results of electron acceleration in ionospheric heating with a spatial scale of kilometers to hundreds of kilometers. The aforementioned model is not self-consistent, and the nonlinear wave–particle interaction has not been discussed in detail. To further investigate these processes, we study the LT numerically with the spatial scale on the order of the Langmuir wave, modeled by the direct kinetic 1 × 1-dimensional (one spatial and one velocity dimension) Vlasov–Poisson system. Another prominent difference between these two models is the electron distribution function, where the Vlasov–Poisson system can show the phase density to lower values to give the time development of electron holes in phase space. The Vlasov

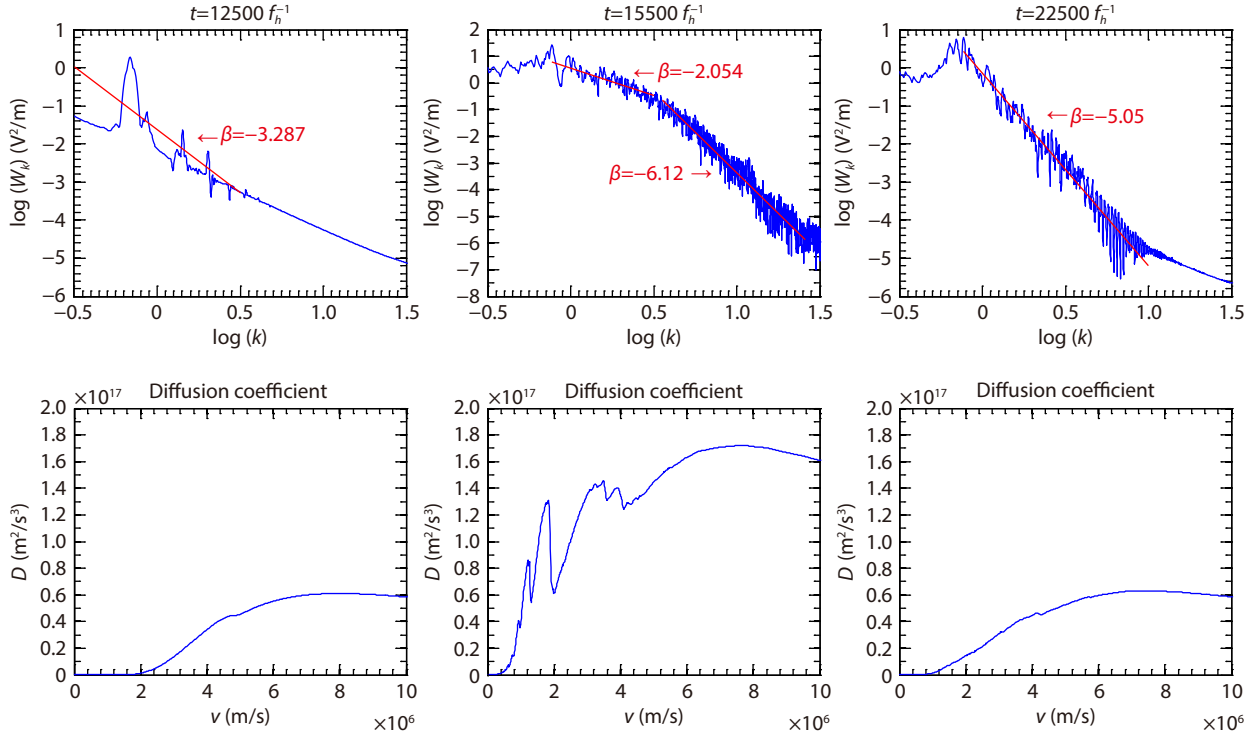

Figure 3. The power spectra (upper panels) and the corresponding diffusion coefficients (lower panels) at the initial parametric decay instability stage, Langmuir turbulence stage, and saturation stage, respectively.

equations of electrons and oxygen ions are as follows:

$$\frac{\partial f_e}{\partial t} + v_e\frac{\partial f_e}{\partial x} - [E_p(t) + E(x,t)]\frac{\partial f_e}{\partial v_e} = 0, \tag{6}$$

$$\frac{\partial f_i}{\partial t} + \sqrt{\mu\alpha}v_i\frac{\partial f_i}{\partial x} + \sqrt{\frac{\mu}{\alpha}}[E_p(t) + E(x,t)]\frac{\partial f_i}{\partial v_i} = 0. \tag{7}$$

By considering the ionospheric component, the oxygen ion is included in this model. The Poisson equation for a self-consistent electric field is as follows:

$$\frac{\partial^2\phi}{\partial x^2} = -(n_i - n_e), \tag{8}$$

$$E = -\frac{\partial\phi}{\partial x}, \tag{9}$$

where f_e (x,v_e,t) and f_i (x,v_i,t) are the electron and ion distribution functions, v_e and v_i are the electron and ion velocities in units (v_{Te}) and (v_{Ti}), respectively, and $v_{Te} = \sqrt{\frac{k_B T_e}{m_e}}$ and $v_{Ti} = \sqrt{\frac{k_B T_i}{m_i}}$ are the electron and ion thermal velocities. The k_B is the Boltzmann constant, T_e and T_i are the initial electron and ion temperatures, m_e and m_i are the electron and ion mass, E (x,t) is the self-consistent electric field in units $\left(\frac{n_0 e}{\varepsilon_0}\lambda_{De}^2\right)$, and $E_p(t)$ is the pump electric field in the same units as $E(x,t)$. The units of time t and space x are f_{pe}^{-1} and λ_{De}, where $f_{pe} = \frac{1}{2\pi}\sqrt{\frac{n_0 e^2}{\varepsilon_0 m_e}}$ is the electron plasma frequency and $\lambda_{De} = \sqrt{\frac{\varepsilon_0 k_B T_e}{n_0 e^2}}$ is the electron Debye length. The parameter μ is the mass ratio defined as $\mu = m_e/m_i$, and α is the temperature ratio defined as $\alpha = T_i/T_e$.

The initial electron and ion temperatures are both chosen as 2,320 K (0.2 eV), and the temperature ratio is $\alpha = 1$. The $n_0 = 1.2705 \times 10^{11}$ el/m^3, which is the same as that in the two-fluid simulation. Thus, the Debye length can be calculated as 0.0093 m. The alternating direction implicit algorithm is used to solve Equations (4) to (7). Periodic boundary conditions are used in space coordinates, and the cutoff boundary is used in velocity space: $f_{e,i}(x, v_{e,i}, t) = 0$, for $v_{e,i} < v_{e,i,\min}$ or $v_{e,i} > v_{e,i,\max}$, where $v_{e,i,\min}$ and $v_{e,i,\max}$ are the cutoff velocities. Here, the $v_{e,i,\min}$ and $v_{e,i,\max}$ are chosen as −35 and 35. The initial electron and ion velocity distributions are assumed to be Maxwell distributions. The initial electron density profile is expressed as $n_{e0}(x) = 1 + 0.001\cos(k_L x)$. The parameter $k_L = 0.03\ \lambda_{De}^{-1}$ is the system wavenumber, which matches the initial Langmuir wave scale in the two-fluid model simulation. The pump electric field is assumed to be uniform in space because the wavelength of the standing wave is much larger than that of Langmuir waves.

Figure 4 presents the time evolution of spectral energy density, the self-consistent electric field energy, the electron and ion temperatures, and the electron and ion velocity distributions in a similar scheme as Figure 2. The main result of Figure 4 is that electron acceleration is accompanied by an increase in Langmuir wave intensity and the extension of wavenumber spectra. Precisely, the E_k is strongly dependent on a prominent extension of the wavenumber spectrum k. When the wavenumber spectrum extends, the electric field energy increases, and the electron temperature then rises with the decrease in the electric field resulting from the wave–particle interaction. Nonlinear Landau damping is the main physical mechanism in this wave–particle interaction. In this case, we observe that the wavenumber spectrum begins to appear at $k = k_L = 0.03$ m^{-1} and extends to larger k. We can also observe two obvious enhanced periods of Langmuir wave intensity, as marked by the two red rectangles in Figure 4. One is at about $t = 8{,}600\ f_h^{-1}$, which is exactly at the beginning of where the spectrum begins to broaden from low k to higher ones. At the same time ($t = 8{,}600\ f_h^{-1}$), the electron temperature edges up slightly. The other enhanced period of Langmuir wave intensity is observed at $t = 12{,}200\ f_h^{-1}$, at which the wavenumber spectrum diffuses to the extensive spectrum range. Meanwhile, the electron temperature increases from 0.5 eV to about 3 eV. However, the Langmuir wave energy at $t = 12{,}200\ f_h^{-1}$ is much smaller than that at $t = 8{,}600\ f_h^{-1}$. Electron acceleration is more effective at $t = 12{,}200\ f_h^{-1}$ than at $t = 8{,}600\ f_h^{-1}$ because the wavenumber spectrum is more wide ranging. The increase in electron temperature is from 0.2 eV to 3.2 eV, whereas that of the ion temperature is from 0.2 eV to 0.21 eV, and the latter is very minute. The complete Landau damping contains an ion contribution. The ion damping at high frequencies is small compared with electronic Landau damping (Baumjohann and Treumann, 2012, Chapter 10). Therefore, the ions are slightly accelerated (the ion temperature increases by less than 5%), as shown in Figure 4d. The time evolution of the electron velocity presents tail acceleration at about $t = 8{,}400\ f_h^{-1}$.

Figure 5 presents the electron hole structures in phase space and the related space average distribution at different times. We can find discrete wavenumbers (namely 2k, 3k, and 4k) of electron holes in phase space at $t = 5{,}000\ f_h^{-1}$, $t = 7{,}500\ f_h^{-1}$, and $t = 7{,}500\ f_h^{-1}$, corresponding to the different velocities ($v_e = \omega/k$, where $k = 2k_L$, $3k_L$, $4k_L$) in the left column of Figure 5. In Figure 5f, the blue line is smooth, suggesting the original state at $t = 0$. The red line ($t =$

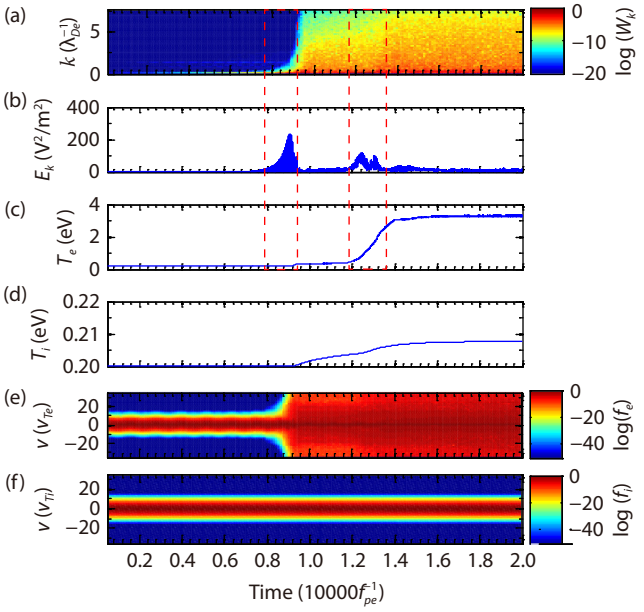

Figure 4. The time evolution of spectral energy density (a), self-consistent electric field energy (b), electron temperature (c), ion temperature (d), electron distribution f_e (e), and ion distribution f_i (f).

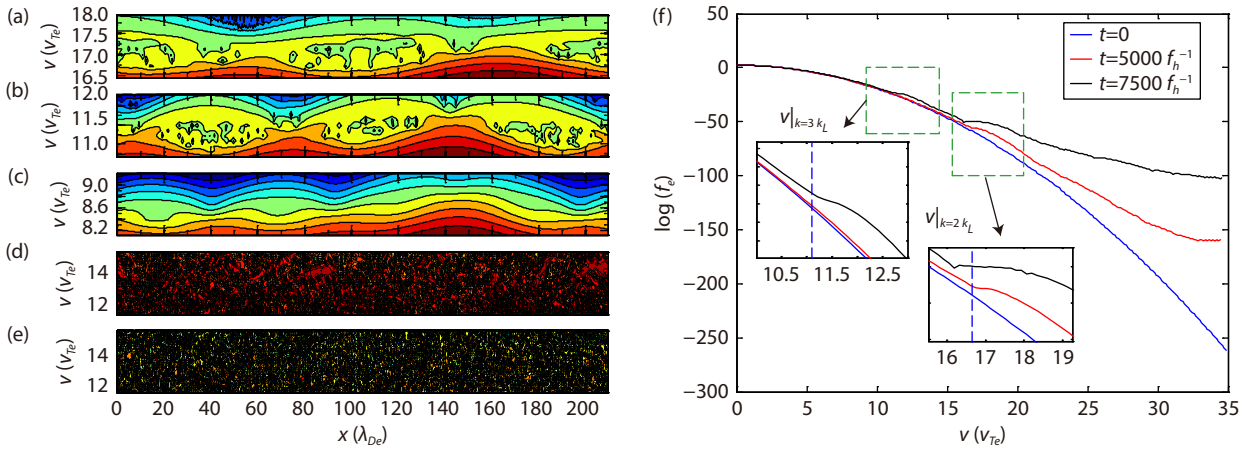

Figure 5. The electron distribution f_e in phase space at t = 5,000 f_h^{-1} (a), t = 7,500 f_h^{-1} (b), t = 7,500 f_h^{-1} (c), t = 8,600 f_h^{-1} (d), and t = 12,500 f_h^{-1} (e). Panel (f) shows the space average distributions at t = 0, t = 5,000 f_h^{-1}, and t = 7,500 f_h^{-1}.

5,000 f_h^{-1}) shows a sudden increase at $k = 2k_L$, consistent with the two electron holes in Figure 5a. The black line likely presents two reflection points ($k = 2k_L$ and $3k_L$) at different velocities (about 11.5 and 16.3), and the three electron holes corresponding to $3k_L$ are shown in Figure 5b. The sudden increase in points of the space average distribution indicates the electrons are being accelerated. Therefore, the electron holes in phase space occurring at different velocities at the same spatial scale as Langmuir waves demonstrate the acceleration of electrons in the initial PDI stage. However, the electron temperature does not increase significantly at the corresponding time in Figure 4 because of wavenumber spectrum enhancements at limited k and the corresponding space average distribution enhancements at limited velocities. At t = 8,600 f_h^{-1} and t = 12,500 f_h^{-1} (Figures 5d and 5e), the electron holes in phase space are explosive, with a scale like that of the wide-ranging Langmuir wavenumbers, and an evident electron temperature enhancement can be observed at the same time in Figure 4. This means that (1) electrons with a definite velocity can be trapped in the hole with the corresponding wavenumber ($k = \omega/v_e$), contributing to the existence of the phase space hole structure at the related time, and (2) the development of the wavenumber spectrum from discrete to continuous because of LT generation is very important for effective electron acceleration.

4. Discussion and Summary

Both the two-fluid model and the Vlasov–Poisson model demonstrate that effective electron acceleration corresponds to a changing of the wavenumber spectrum, which means that the generation of LT is very important in the process. The results of the two-fluid simulation present the PDI generation and caviton formation. The velocity distribution of electrons calculated by the Fokker–Planck equation, which is based on the results of the two-fluid model, helps describe the time evolution of electron acceleration by LT. However, the simulation results of the Vlasov–Poisson model present the dynamics of electron acceleration in detail. The collapse and nucleation of cavitons can lead to an extension of the wavenumber spectrum (Doolen et al., 1985). Meanwhile, the electric field energy increases, and the electron temperature then rises with the decrease in the electric field because of the wave–particle interaction, in which nonlinear Landau damping is the main physical mechanism. When a wave develops into a large-amplitude wave, collisionless damping with trapping does occur. The amplitude of the wave fluctuates during the decay as the trapped particles bounce back and forth in the potential wells (Chen FF, 1984). These trapped electrons contribute to the occurrence of electron holes in phase space, with scales like the corresponding Langmuir wavenumbers. The electron holes in phase space are excited at different velocities, and the related space average distribution increases at the corresponding velocity, revealing the acceleration of electrons. The increasing wide-ranging wavenumber spectrum in strong LT may give rise to the number of electron holes in phase space at greater velocities, which results in further acceleration of electrons.

In general, our results support the formation of LT, in which the electrons are more effectively accelerated and more electron holes exist at related velocities; thus, this process is important for electron acceleration in ionospheric heating. Moreover, the simulation results could be beneficial for understanding the physical process of electron acceleration during ionospheric heating experiments.

Acknowledgments

This work was supported by the National Natural Science Foundation of China (NSFC Grant Nos. 42104150, 42074187, 41774162, and 41704155), the Foundation of the National Key Laboratory of Electromagnetic Environment (Grant No. 6142403200303), the Chinese Academy of Sciences, Key Laboratory of Geospace Environment, the University of Science & Technology of China (Grant No. GE2020-01), the Fundamental Research Funds for the Central Universities (Grant No. 2042021kf0020), and the Excellent Youth Foundation of Hubei Provincial Natural Science Foundation (Grant No. 2019CFA054). Electron acceleration data are available in the Zenodo repository (http://doi.org/10.5281/zenodo.4098938).

References

Baumjohann, W., and Treumann, R. A. (2012). *Basic Space Plasma Physics*. London: Imperial College Press.

Bryers, C. J., Kosch, M. J., Senior, A., Rietveld, M. T., and Yeoman, T. K. (2013). The

thresholds of ionospheric plasma instabilities pumped by high-frequency radio waves at EISCAT. *J. Geophys. Res.: Space Phys.*, *118*(11), 7472–7481. https://doi.org/10.1002/2013JA019429

Carlson, H. C., Gordon, W. E., and Showen, R. L. (1972). High frequency induced enhancements of the incoherent scatter spectrum at Arecibo. *J. Geophys. Res.*, *77*(7), 1242–1250. https://doi.org/10.1029/JA077i007p01242

Chen, F. F. (1984). *Introduction to Plasma Physics and Controlled Fusion*. New York: Plenum Press.

Dang, T., Lei, J. H., Dou, X. K., and Wan, W. X. (2017). A simulation study of 630 nm and 557.7 nm airglow variations due to dissociative recombination and thermal electrons by high-power HF heating. *Earth Planet. Phys.*, *1*, 44–52. https://doi.org/10.26464/epp2017006

Djuth, F. T., Bernhardt, P. A., Tepley, C. A., Gardner, J. A., Kelley, M. C., Broadfoot, A. L., Kagan, L. M., Sulzer, M. P., Elder, J. H., … Carlson, H. C. (1999). Large airglow enhancements produced via wave-plasma interactions in sporadic E. *Geophys. Res. Lett.*, *26*(11), 1557–1560. https://doi.org/10.1029/1999GL900296

Djuth, F. T., Pedersen, T. R., Gerken, E. A., Bernhardt, P. A., Selcher, C. A., Bristow W. A., and Kosch M. J. (2005). Ionospheric modification at twice the electron cyclotron frequency. *Phys. Rev. Lett.*, *94*(12), 125001. https://doi.org/10.1103/PhysRevLett.94.125001

Doolen, G. D., DuBois, D. F., and Rose, H. A. (1985). Nucleation of cavitons in strong Langmuir turbulence. *Phys. Rev. Lett.*, *54*(8), 804–807. https://doi.org/10.1103/PhysRevLett.54.804

DuBois, D. F., Rose, H. A., and Russell, D. (1988). Power spectra of fluctuations in strong Langmuir turbulence. *Phys. Rev. Lett.*, *61*(19), 2209–2212. https://doi.org/10.1103/PhysRevLett.61.2209

Eliasson, B. (2008). Full-scale simulation study of the generation of topside ionospheric turbulence using a generalized Zakharov model. *Geophys. Res. Lett.*, *35*(11), L11104. https://doi.org/10.1029/2008GL033866

Eliasson, B., Shao, X., Milikh, G., Mishin, E. V., and Papadopoulos, K. (2012). Numerical modeling of artificial ionospheric layers driven by high-power HF heating. *J. Geophys. Res.: Space Phys.*, *117*(A10), A10321. https://doi.org/10.1029/2012JA018105

Eliasson, B., and Shukla, P. K. (2004). Trapping of Langmuir waves in ion holes. *Phys. Scr.*, *2004*(T107), 192. https://doi.org/10.1238/Physica.Topical.107a00192

Eliasson, B., and Shukla, P. K. (2006). Formation and dynamics of coherent structures involving phase-space vortices in plasma. *Phys. Rep.*, *422*(6), 225–290. https://doi.org/10.1016/j.physrep.2005.10.003

Eliasson, B., and Stenflo, L. (2008). Full-scale simulation study of the initial stage of ionospheric turbulence. *J. Geophys. Res.: Space Phys.*, *113*(A2), A02305. https://doi.org/10.1029/2007JA012837

Fejer, J. A. (1979). Ionospheric modification and parametric instabilities. *Rev. Geophys.*, *17*(1), 135–153. https://doi.org/10.1029/RG017i001p00135

Feng, T., Zhou, C., Wang, X., Liu, M. R., and Zhao, Z. Y. (2020). Evidence of X-mode heating suppressing O-mode heating. *Earth Planet. Phys.*, *4*(6), 588–597. https://doi.org/10.26464/epp2020068

Hanssen, A., Mjølhus, E., DuBois, D. F., and Rose, H. A. (1992). Numerical test of the weak turbulence approximation to ionospheric Langmuir turbulence. *J. Geophys. Res.: Space Phys.*, *97*(A8), 12073–12091. https://doi.org/10.1029/92JA00874

Isham, B., La Hoz, C., Rietveld, M. T., Hagfors, T., and Leyser, T. B. (1999). Cavitating Langmuir turbulence observed during high-latitude ionospheric wave interaction experiments. *Phys. Rev. Lett.*, *83*(13), 2576–2579. https://doi.org/10.1103/PhysRevLett.83.2576

Mishin, E., Watkins, B., Lehtinen, N., Eliasson, B., Pedersen, T., and Grach, S. (2016). Artificial ionospheric layers driven by high-frequency radiowaves: an assessment. *J. Geophys. Res.: Space Phys.*, *121*(4), 3497–3524. https://doi.org/10.1002/2015JA021823

Najmi, A., Eliasson, B., Shao, X., Milikh, G., Sharma, A. S., and Papadopoulos, K. (2017). Vlasov simulations of electron acceleration by radio frequency heating near the upper hybrid layer. *Phys. Plasmas*, *24*(10), 102904. https://doi.org/10.1063/1.4999768

Perkins, F. W., Oberman, C., and Valeo, E. J. (1974). Parametric instabilities and ionospheric modification. *J. Geophys. Res.*, *79*(10), 1478–1496. https://doi.org/10.1029/JA079i010p01478

Robinson, T. R. (1989). The heating of the high lattitude ionosphere by high power radio waves. *Phys. Rep.*, *179*(2–3), 79–209. https://doi.org/10.1016/0370-1573(89)90005-7

Sergeev, E., Grach, S., Shindin, A., Mishin, E., Bernhardt, P., Briczinski, S., Isham, B., Broughton, M., LaBelle, J., and Watkins, B. (2013). Artificial ionospheric layers during pump frequency stepping near the 4th gyroharmonic at HAARP. *Phys. Rev. Lett.*, *110*(6), 065002. https://doi.org/10.1103/PhysRevLett.110.065002

Thidé, B., Kopka, H., and Stubbe, P. (1982). Observations of stimulated scattering of a strong high-frequency radio wave in the ionosphere. *Phys. Rev. Lett.*, *49*(21), 1561–1564. https://doi.org/10.1103/PhysRevLett.49.1561

Wang, X., Zhou, C., Xu, T., Honary, F., Rietveld, M., and Frolov, V. (2019). Stimulated electromagnetic emissions spectrum observed during an X-mode heating experiment at the European Incoherent Scatter Scientific Association. *Earth Planet. Phys.*, *3*(5), 391–399. https://doi.org/10.26464/epp2019042

Weinstock, J. (1975). Theory of enhanced airglow during ionospheric modifications. *J. Geophys. Res.*, *80*(31), 4331–4345. https://doi.org/10.1029/JA080i031p04331

Weinstock, J., and Bezzerides, B. (1974). Theory of electron acceleration during parametric instabilities. *Phys. Rev. Lett.*, *32*(14), 754–758. https://doi.org/10.1103/PhysRevLett.32.754